Hindawi Publishing Corporation
Mathematical Problems in Engineering
Volume 2015, Article ID 104041, 9 pages
http://dx.doi.org/10.1155/2015/104041

Research Article

Modeling of Acceleration Influence on Hemispherical Resonator Gyro Forcing System

Guoxing Yi,[1] Yangguang Xie,[2] Ziyang Qi,[1] and Boqi Xi[1]

[1] *Space Control and Inertial Technology Research Center, Harbin Institute of Technology, Harbin 150001, China*
[2] *Flight Automatic Control Research Institute, Aviation Industry Corporation of China, Xi'an 710065, China*

Correspondence should be addressed to Guoxing Yi; ygx@hit.edu.cn

Received 5 June 2014; Accepted 20 September 2014

Academic Editor: Minrui Fei

Acceleration adds negative effect to Hemispherical Resonator Gyro (HRG) output; therefore, it is important to model the influence and then make necessary compensations, accordingly. Based on the elastic thin-shell theory under the Kirchhoff-Love assumption, the acceleration influence on HRG forcing system is modeled and then schemes for incentive are suggested. Firstly, the dynamic model of resonator is introduced. Then, inertial load and electrostatic force are calculated to obtain the deformation of resonator. At last, schemes for pickoff incentive are proposed to weaken the effect of acceleration on HRG forcer. The simulation results illustrate that acceleration has negative effects on the exciting confidents of forcers and the proposed scheme can eliminate the acceleration influence on forcing system.

1. Introduction

The hemispherical resonator gyro (HRG) is a solid state gyroscope whose sensing property is based on the vibration structure. It has the features of high accuracy, long life span, inherent high reliability, natural radiation hardness, and no parts that can wear out, which makes it very suitable for applications in long-time working state such as in space vehicles [1–4]. Particularly, over 125 spacecraft missions whose Space Inertial Reference Unit (SIRU) is based on HRGs have been launched successfully by NASA, Department of Defense (DOD) and so on. Moreover, it is reported that HRGs have already achieved 18 million h of continuous operation with 100 percent mission success in space application.

In the practical use of HRG, acceleration will have inevitable effects on the HRG, which also can increase the gyro drift. As a kind of high precision gyro, the drift caused by acceleration is not allowable to be ignored. So the research on the drift caused by the accelerations has important practical application value.

The HRG contains three primary functional components: the hemispherical resonator, the forcer, and the pickoff. According to the elastic thin-shell theory under the Kirchhoff-Love assumption [5], under the action of acceleration, the resonator will produce a large deformation, causing the change of relative position between resonator and the exciting electrode, which inevitably impacts on internal control system of HRG. Zhou et al. [6] provided some acceleration consequence analysis of HRG based on experiments. Zhbanov [7–9] discussed the effect of movability of the resonator center excited by an electrostatic field. Watson [10] studied on the driver geometry of skewed pick-off. Forcer is the "actuator" of the internal control system of HRG. The resonator's deformation will increase the errors in the excitation system, which is an important part of gyro's drift of HRG, so the influence of resonator deformation caused by acceleration on forcing system will be discussed in this paper.

2. Dynamic Characteristics of Resonator

2.1. Dynamic Model of Resonator. Acquiring from the elastic thin-shell theory, under the Kirchhoff-Love assumption, shell satisfies the force balance equation, the geometric equation of deformation and displacement, and the elastic equation. Synthesizing the three equations, the differential equations of the shell's middle surface can be set in

the domain of shell, under the given boundary conditions; the distribution of displacement field or the force field can be obtained by solving the differential equations within the domain.

In the process of modeling, the structure of an umbrella-type resonator whose radius is R and thickness is $2h$ can be simplified as hemispherical and be modeled; then the hemispherical latitude line θ and longitude line φ constitute the principal coordinate system, as shown in Figure 1; the differential equation to establish the displacement components is shown as follows:

$$\begin{aligned}
&D\left[\frac{\partial^3 w}{\partial\theta^3}+\frac{\mu}{\sin^2\theta}\frac{\partial^3 w}{\partial\theta\partial\varphi^2}+\frac{\cos\theta}{\sin\theta}\frac{\partial^2 w}{\partial\theta^2}\right.\\
&\quad\left.+\frac{-\cos\theta-\mu\cos\theta}{\sin^3\theta}\frac{\partial^2 w}{\partial\varphi^2}+\frac{\sin^2\theta-\cos^2\theta}{\sin^2\theta}\frac{\partial w}{\partial\theta}\right]\\
&\quad+D_1\left[\frac{1}{\sin^2\theta}\frac{\partial^3 w}{\partial\theta\partial\varphi^2}-\frac{\cos\theta}{\sin^3\theta}\frac{\partial^2 w}{\partial\varphi^2}\right]=R^4X,\\
&D\left[\frac{\partial^3 w}{\partial\varphi^3}\frac{1}{\sin^3\theta}+\frac{\mu}{\sin\theta}\frac{\partial^3 w}{\partial\theta^2\partial\varphi}+\frac{\cos\theta}{\sin^2\theta}\frac{\partial^2 w}{\partial\theta\partial\varphi}\right.\\
&\quad\left.+\frac{(1+\mu)}{\sin\theta}\frac{\partial w}{\partial\varphi}\right]\\
&\quad+D_1\left[\frac{1}{\sin\theta}\frac{\partial^3 w}{\partial\theta^2\partial\varphi}+\frac{1}{\sin\theta}\frac{\partial w}{\partial\varphi}\right]=R^4Y,\\
&D\left[\frac{\partial^4 w}{\partial\theta^4}+\frac{1}{\sin^4\theta}\frac{\partial^4 w}{\partial\varphi^4}+\frac{2\mu}{\sin^2\theta}\frac{\partial^4 w}{\partial\theta^2\partial\varphi^2}\right.\\
&\quad+\frac{2\cos\theta}{\sin\theta}\frac{\partial^3 w}{\partial\theta^3}-\frac{2\mu\cos\theta}{\sin^3\theta}\frac{\partial^3 w}{\partial\theta\partial\varphi^2}-\frac{\cos^2\theta}{\sin^2\theta}\frac{\partial^2 w}{\partial\theta^2}\\
&\quad\left.+\frac{2+2\mu}{\sin^4\theta}\frac{\partial^2 w}{\partial\varphi^2}+\left(\frac{2\cos\theta}{\sin\theta}+\frac{\cos\theta}{\sin^3\theta}\right)\frac{\partial w}{\partial\theta}\right]\\
&\quad+D_1\left[\frac{2}{\sin^2\theta}\frac{\partial^4 w}{\partial\theta^2\partial\varphi^2}-\frac{2\cos\theta}{\sin^3\theta}\frac{\partial^3 w}{\partial\theta\partial\varphi^2}\right.\\
&\quad\left.+\frac{2}{\sin^4\theta}\frac{\partial^2 w}{\partial\varphi^2}\right]=R^2Z,
\end{aligned}\tag{1}$$

where w is defined as a spherical point P that moves to P' for the spherical deformation, deriving the displacement vector $\mathbf{U}$, and the projections on the local frame $\boldsymbol{\rho}_1\boldsymbol{\rho}_2\mathbf{n}$ are u, v, w, respectively, in which w is the normal displacement, shown in Figure 1; R is the radius of middle surface of spherical shell; $N = 2Eh/(1-\mu^2)$; $N_1 = Eh/(1+\mu)$; $D = 2Eh^3/3(1-\mu^2)$; $D_1 = 2Eh^3/3(1+\mu)$; E is Young's modulus; μ is Poisson ratio; X, Y, and Z are the projections of external load (the distributed force) on $\boldsymbol{\rho}_1\boldsymbol{\rho}_2\mathbf{n}$.

It can be seen from (1) that, under the function of additive loads, the equation meets the superposition principle. The external loads discussed in the paper include inertial load and the electrostatic force of exciter.

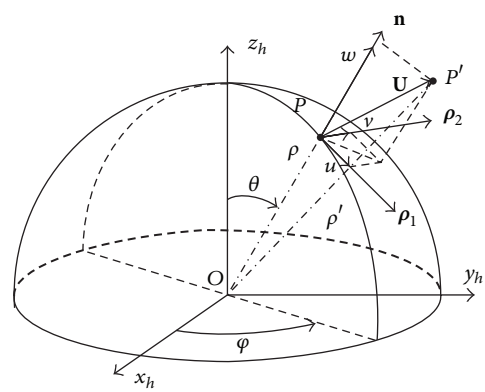

Figure 1: Schematic diagram of resonator.

2.2. Inertial Load. Inertial force of spherical shell is an important part of the external loads, and the gyroscopic effect of oscillator is embodied through the item. Acceleration expression of any material point on oscillator relative to the inertial space is

$$\mathbf{a}_i=\mathbf{a}_{ih}+\left.\frac{d^2\mathbf{U}}{dt^2}\right|_c+2\boldsymbol{\omega}_{ic}\times\left.\frac{d\mathbf{U}}{dt}\right|_c,\tag{2}$$

where $\mathbf{a}_{ih}$ is the acceleration of resonator coordinate system relative to inertial coordinate system; $\boldsymbol{\omega}_{ic}$ is the rotation angular rate of the local frame $\boldsymbol{\rho}_1\boldsymbol{\rho}_2\mathbf{n}$ relative to the inertial coordinate system. Because $\boldsymbol{\rho}_1\boldsymbol{\rho}_2\mathbf{n}$ is static relative to the resonator coordinate system, $\boldsymbol{\omega}_{ic}$ is also the rotation angular rate of resonator coordinate system relative to inertial coordinate system which is described as $\boldsymbol{\omega}_{ih}$.

The types of components of the vectors in (2) in the local frame are expressed as

$$\begin{aligned}
\mathbf{a}_i&=\left[a_{ix}^c\quad a_{iy}^c\quad a_{iz}^c\right]^T,\\
\mathbf{a}_{ih}&=\left[a_{ihx}^c\quad a_{ihy}^c\quad a_{ihz}^c\right]^T\\
&=\begin{bmatrix}\cos\theta\cos\varphi & \cos\theta\sin\varphi & -\sin\theta\\ -\sin\varphi & \cos\varphi & 0\\ \sin\theta\cos\varphi & \sin\theta\sin\varphi & \cos\theta\end{bmatrix}\begin{bmatrix}a_{ihx}^h\\ a_{ihy}^h\\ a_{ihz}^h\end{bmatrix},\\
\left.\frac{d\mathbf{U}}{dt}\right|_c&=\left[\frac{du}{dt}\quad\frac{dv}{dt}\quad\frac{dw}{dt}\right]^T,\\
\left.\frac{d^2\mathbf{U}}{dt^2}\right|_c&=\left[\frac{d^2u}{dt^2}\quad\frac{d^2v}{dt^2}\quad\frac{d^2w}{dt^2}\right]^T,\\
\boldsymbol{\omega}_{ih}&=\left[\omega_{ihx}^h\quad\omega_{ihy}^h\quad\omega_{ihz}^h\right]^T,
\end{aligned}\tag{3}$$

where a_{ix}^c, a_{iy}^c, and a_{iz}^c are the acceleration components of material point of harmonic point relative to inertial coordinate system in the local frame, respectively; a_{ihx}^h, a_{ihy}^h, and a_{ihz}^h are components of the acceleration of the resonator coordinate system relative to inertial coordinate system in the resonator coordinate system, respectively. ω_{ihx}^h, ω_{ihy}^h, and

ω_{ihz}^{h} are the components of angular rate of the resonator coordinate system relative to inertial coordinate system in the resonator coordinate system, respectively.

Because (1) satisfies the superposition principle, the inertial load can be divided into two conditions in this paper.

The first condition is the consideration of the function of external low-frequency acceleration $\mathbf{a}_{ih}$ as well as the deformation of resonator $d^2\mathbf{U}/dt^2|_c$ caused by $\mathbf{a}_{ih}$, namely,

$$\mathbf{a}_i = \mathbf{a}_{ih} + \left.\frac{d^2\mathbf{U}}{dt^2}\right|_c. \tag{4}$$

The second condition is the inconsideration of $\mathbf{a}_{ih}$ in the state of second-order vibration of resonator; meanwhile (2) can be simplified as

$$\mathbf{a}_i = \left.\frac{d^2\mathbf{U}}{dt^2}\right|_c + 2\boldsymbol{\omega}_{ic} \times \left.\frac{d\mathbf{U}}{dt}\right|_c. \tag{5}$$

2.3. Electrostatic Force. The structure of polar plate of actuator on external base of HRG is spherical sector, shown as Figure 2. θ_{ab}, θ_{at} are the latitude ranges of the spherical sector and $\varphi_{al}, \varphi_{ar}$ are the longitude ranges of the sector.

The frequency of the control alternating current voltage is the half of the second order resonance frequency of resonator. The expression of the AC voltage is:

$$V(\theta,\varphi,t) = \begin{cases} 0 & \text{else} \\ V_0 \cos\left(\dfrac{\omega_2 t}{2}\right) & \theta_{at} \le \theta \le \theta_{ab}, \varphi_{al} \le \varphi \le \varphi_{ar}. \end{cases} \tag{6}$$

Because the capacitance clearance is in micron level, which is small relative to the resonator radius, so the spherical curvature can be ignored, the exciter can be treated as plate-type capacitor, and the boundary effect is ignored at the same time. The expression of electric field force (surface force) acting to the resonator can be expressed as

$$q = -\frac{\varepsilon_0 V^2}{2d^2} = -\frac{\varepsilon_0 V_0^2}{2d^2} f(\varphi,\theta) \cos^2\frac{\omega_2 t}{2}, \tag{7}$$

where

$$f(\varphi,\theta) = \begin{cases} 0 & \text{else} \\ 1 & \theta_{at} \le \theta \le \theta_{ab},\ \varphi_{al} \le \varphi \le \varphi_{ar}. \end{cases} \tag{8}$$

Ignoring the constant of the electric field force, (7) can be formed as

$$q = -\frac{\varepsilon_0 V_0^2}{4d^2} f(\varphi,\theta) \cos\omega_2 t. \tag{9}$$

The effecting direction of electric field force is the normal direction of the outside surface of resonator. When resonator is under the condition of vibration, because the vibration contains the tangential motion, the normal direction of the outside surface of resonator varies constantly, leading to the existence of tangential component. While the amplitude of resonator is small compared to the radius, the tangential component can be negligible and the normal component of electric field force can be approximately taken as (9).

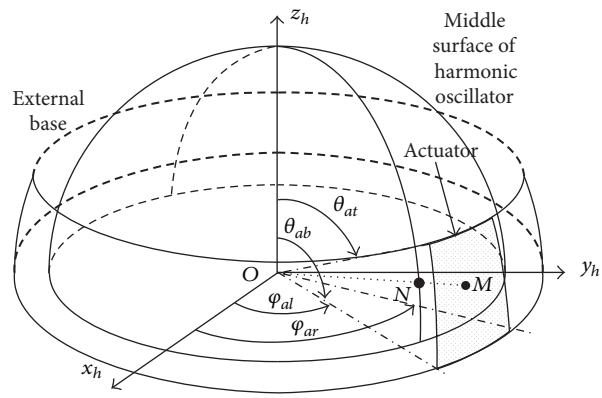

Figure 2: Structure diagram of vibration pickup.

3. Multielectrode Incentive Features

3.1. Actuator Configuration Structure. The external base of HRG uniformly distributes 16 exciter, and the interval is 22.5°, presented as F_1~F_{16} as shown in Figure 3. The longitude and latitude ranges of electrode are shown in Table 1. Typically, the exciter in position of wave amplitude of resonator actuator can be used in amplitude vibration and amplitude stability and electrode of node can be used for rate feedback. According to the symmetry of the second-order resonance state of resonator, 16 exciters can construct the following three kinds of structure forms.

(1) F_1 at 0° of electrode axis is taken as exciter for amplitude stability, and F_3 at 45° of electrode axis is taken as exciter for force feedback. As shown in Figure 3, this is the most basic form of testing structure, defined as Scheme a.

(2) F_1 and F_5 are paralleled as the exciter for amplitude stability. F_2 and F_6 are paralleled as exciter for force feedback, shown as Figure 3, which is defined as Scheme b.

(3) F_1, F_9, F_5, and F_{13} are taken as exciter for amplitude stability, $V_a \cos\omega_2 t$ AC voltage is exerted on F_1, F_9, and $-V_a \cos\omega_2 t$ AC voltage is exerted on F_5, F_{13}. F_3, F_{11}, F_7, and F_{15} are taken as exciter for amplitude stability, $V_m \cos\omega_2 t$ AC voltage is exerted on F_3, F_{11}, and $-V_m \cos\omega_2 t$ AC voltage is exerted on F_7, F_{15} shown as Figure 3(c) and defined as Scheme c.

3.2. Exciter Characteristics. As Figure 2 showed, in the condition of existence of electrode excitements, X, Y, and Z in components of external load in (1) can be expressed as

$$\begin{aligned} X &= -\rho h a_{ix}^c, \\ Y &= -\rho h a_{iy}^c, \\ Z &= -\rho h a_{iz}^c + q. \end{aligned} \tag{10}$$

Substituting it into (1), the vibration equation can be complied under the effect of single exciter of resonator.

Table 1: Electrode range.

Name	Parameter value	Name	Parameter value	Name	Parameter value	Name	Parameter value
θ_{abi} $i = 1, 2, \ldots, 16$	85°	θ_{ati} $i = 1, 2, \ldots, 16$	75°	φ_{al8}	147.5°	φ_{ar8}	167.5°
				φ_{al9}	170°	φ_{ar9}	190°
φ_{al1}	350°	φ_{ar1}	10°	φ_{al10}	192.5°	φ_{ar10}	212.5°
φ_{al2}	12.5°	φ_{ar2}	32.5°	φ_{al11}	215°	φ_{ar11}	235°
φ_{al3}	35°	φ_{ar3}	55°	φ_{al12}	237.5°	φ_{ar12}	257.5°
φ_{al4}	57.5°	φ_{ar4}	77.5°	φ_{al13}	260°	φ_{ar13}	280°
φ_{al5}	80°	φ_{ar5}	100°	φ_{al14}	282.5°	φ_{ar14}	302.5°
φ_{al6}	102.5°	φ_{ar6}	122.5°	φ_{al15}	305°	φ_{ar15}	325°
φ_{al7}	125°	φ_{ar7}	145°	φ_{al16}	327.5°	φ_{ar16}	347.5°

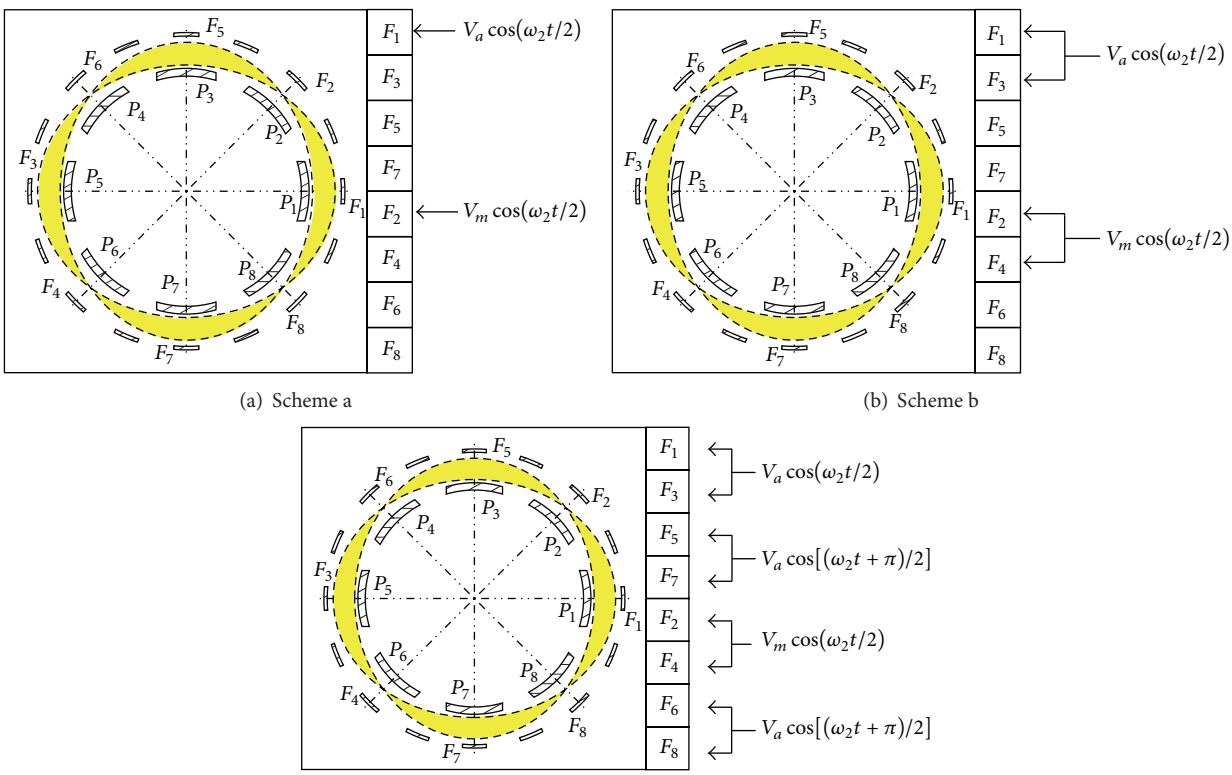

(a) Scheme a

(b) Scheme b

(c) Scheme c

Figure 3: Structure diagram of exciter.

While the form of the analytical solution of the state equation of second-order harmonic vibration of resonator is

$$\begin{bmatrix} u_2 \\ v_2 \\ w_2 \end{bmatrix} = \begin{bmatrix} U_2 \cos 2\varphi \\ V_2 \sin 2\varphi \\ W_2 \cos 2\varphi \end{bmatrix} p(t) + \begin{bmatrix} U_2 \sin 2\varphi \\ -V_2 \cos 2\varphi \\ W_2 \sin 2\varphi \end{bmatrix} q(t), \quad (11)$$

where $p(t)$, $q(t)$ are undetermined variables related to time and U_2, V_2, and W_2 are Rayleigh Functions, the form is as follows:

$$U_2 = V_2 = \sin\theta \tan^2 \frac{\theta}{2}, \qquad W_2 = -(2 + \cos\theta) \tan^2 \frac{\theta}{2}. \quad (12)$$

When the dynamic equation and the analytical solution form are known, a method of solving the equation's approximate solution is to use Bubnov-Galerkin method. Eventually the undetermined variables $p(t)$ and $q(t)$ in (11) can be obtained that they meet the second-order differential equation. Substituting damping coefficient ξ_2 into the equation, it can be formed as

$$\ddot{p}(t) + \omega_2^2 \xi_2 \dot{p}(t) - 4K\Omega \dot{q}(t) + \omega_2^2 p(t) = -(H_a K_{c0} + H_m K_{c45}) \cos \omega_2 t,$$

$$\ddot{q}(t) + \omega_2^2 \xi_2 \dot{q}(t) + 4K\Omega \dot{p}(t) + \omega_2^2 q(t) = -\left(H_a K_{s0} + H_m K_{s45}\right) \cos \omega_2 t, \tag{13}$$

where

$$H_a = \frac{\varepsilon_0 R^2 V_a^2}{4m_0}, \qquad H_m = \frac{\varepsilon_0 R^2 V_m^2}{4m_0}. \tag{14}$$

When the excitement mode is taken as Scheme a,

$$\begin{aligned} K_{c0} &= K_{c1}, \qquad K_{c45} = K_{c2}, \\ K_{s0} &= K_{s1}, \qquad K_{s45} = K_{s2}. \end{aligned} \tag{15}$$

When the excitement mode is taken as Scheme b,

$$\begin{aligned} K_{c0} &= K_{c1} + K_{c3}, \qquad K_{c45} = K_{c2} + K_{c4}, \\ K_{s0} &= K_{s1} + K_{s3}, \qquad K_{s45} = K_{s2} + K_{s4}. \end{aligned} \tag{16}$$

When the excitement mode is taken as Scheme c,

$$\begin{aligned} K_{c0} &= K_{c1} + K_{c3} - K_{c5} - K_{c7}, \\ K_{c45} &= K_{c2} + K_{c4} - K_{c6} - K_{c8}, \\ K_{s0} &= K_{s1} + K_{s3} - K_{s5} - K_{s7}, \\ K_{s45} &= K_{s2} + K_{s4} - K_{s6} - K_{s8}, \end{aligned} \tag{17}$$

where

$$\begin{aligned} K_{ci} &= \int_{\varphi_{ali}}^{\varphi_{ari}} \int_{\theta_{ati}}^{\theta_{abi}} \frac{W(\theta) \sin\theta \cos 2\varphi}{d^2} \, d\theta \, d\varphi, \\ K_{si} &= \int_{\varphi_{ali}}^{\varphi_{ari}} \int_{\theta_{ati}}^{\theta_{abi}} \frac{W(\theta) \sin\theta \sin 2\varphi}{d^2} \, d\theta \, d\varphi, \\ & \qquad i = 1, 2, \ldots, 8. \end{aligned} \tag{18}$$

Then,

$$\begin{aligned} \omega_2^3 \xi_2 m - 4K\Omega n \omega_2 &= -\left(H_a K_{c0} + H_m K_{c45}\right), \\ \omega_2^3 \xi_2 n + 4K\Omega m \omega_2 &= -\left(H_a K_{s0} + H_m K_{s45}\right), \end{aligned} \tag{19}$$

$$\Omega = \frac{\omega_2^2 \xi_2}{4K} \tan\left[\arctan \frac{H_a K_{c0} + H_m K_{c45}}{H_a K_{s0} + H_m K_{s45}} - 2\vartheta\right]. \tag{20}$$

For further discussion of the exciting features, Scheme a is taken as an example to explain, ignoring the structure error of HRG. Substitute the data in Table 1 into the equation:

$$\Omega = \frac{\omega_2^2 \xi_2}{4K} \tan\left\{\arctan \frac{H_m}{H_a} - 2\vartheta\right\}. \tag{21}$$

Seen from the equation above, appropriate H_m, H_a can be found to make $\vartheta = 0$; when $n = 0$ in (19), (19) can be simplified as

$$\begin{aligned} m &= -\frac{K_{c1} H_a}{\omega_2^3 \xi_2}, \\ \Omega &= -\frac{K_{s2} H_m}{4K m \omega_2}. \end{aligned} \tag{22}$$

When the vibration mode angle of resonator is locked at zero, the above two equations represent the rules for amplitude control and control link of the vibration mode angle. It can be seen that the two control loops are no coupling, but actually because of factors such as errors of form and position and deformation, the two loops are coupling, and the coupling relationship can be described by (19). In the process of gyro design, make sure to avoid coupling of two control loops to the greatest extent; namely, the aim $K_{c0} = K_{s45} = 0$ comes true and K_{c45}, K_{s0} are constants.

4. Deformation Caused by Acceleration

As shown in Figure 2, take any point M within the scope of exciter area. Line OM intersects with the middle surface after the deformation of resonator at point N, where $OM = R_{in}$; suppose $ON = R_d$, and the expression of capacitance clearance is

$$d = R_{in} - R_d - h. \tag{23}$$

In order to solve R_d in the above equation, the surface equation after deformation should be known. As shown in Figure 2, the material point P in the middle surface of resonator moves to point P' after deformation, the displacement vector ρ' corresponds to P' and ρ corresponds to P, and the deformation vector has the relationship as follows:

$$\rho' = \rho + \mathbf{U}. \tag{24}$$

And the component form in the resonator coordinate system $x_h y_h z_h$ is

$$\begin{bmatrix} x \\ y \\ z \end{bmatrix} = R \begin{bmatrix} \sin\theta\cos\varphi \\ \sin\theta\sin\varphi \\ \cos\theta \end{bmatrix} + \begin{bmatrix} \cos\theta\cos\varphi & -\sin\varphi & \sin\theta\cos\varphi \\ \cos\theta\sin\varphi & \cos\varphi & \sin\theta\sin\varphi \\ -\sin\theta & 0 & \cos\theta \end{bmatrix} \begin{bmatrix} u \\ v \\ w \end{bmatrix}, \tag{25}$$

where u, v, and w include the deformation caused by acceleration u_1, v_1, w_1 and u_2, v_2, w_2 when resonator steps into second-order state.

The intersection between Line OM and the middle surface of resonator meets the equation as follows:

$$R_d \begin{bmatrix} \sin\hat{\theta}\cos\hat{\varphi} \\ \sin\hat{\theta}\sin\hat{\varphi} \\ \cos\hat{\theta} \end{bmatrix} = R \begin{bmatrix} \sin\theta\cos\varphi \\ \sin\theta\sin\varphi \\ \cos\theta \end{bmatrix} + \begin{bmatrix} \cos\theta\cos\varphi & -\sin\varphi & \sin\theta\cos\varphi \\ \cos\theta\sin\varphi & \cos\varphi & \sin\theta\sin\varphi \\ -\sin\theta & 0 & \cos\theta \end{bmatrix} \times \begin{bmatrix} u_1 + u_2 \\ v_1 + v_2 \\ w_1 + w_2 \end{bmatrix}, \tag{26}$$

where $\widehat{\theta}$, $\widehat{\varphi}$ are the latitude and the longitude of the base polar plate in vibration pickup, $\widehat{\theta} \in [\theta_{vt}, \theta_{vb}]$, $\widehat{\varphi} \in [\varphi_{vl}, \varphi_{vr}]$ are known variables, and R_d, θ, and φ are unknown variables.

The deformations u_1, v_1, and w_1 in (26) are shown in (29) and the deformations u_2, v_2, and w_2 in (29) are shown as follows:

$$\begin{bmatrix} u_2 \\ v_2 \\ w_2 \end{bmatrix} = A_a \begin{bmatrix} U_2 \cos 2(\varphi - \vartheta) \\ V_2 \sin 2(\varphi - \vartheta) \\ W_2 \cos 2(\varphi - \vartheta) \end{bmatrix} \sin \omega_2 t, \tag{27}$$

where A_a is the amplitude; ω_2 is the frequency of second-order harmonic vibration of resonator; t is the time; ϑ is vibration mode angle; U_2, V_2, and W_2 are Rayleigh Functions, the form of which is shown as follows:

$$\begin{aligned} U_2 = V_2 &= \sin\theta \tan^2 \frac{\theta}{2}, \\ W_2 &= -(2 + \cos\theta) \tan^2 \frac{\theta}{2}. \end{aligned} \tag{28}$$

The form of deformation equation under the effect of resonator is

$$\begin{bmatrix} u_1 \\ v_1 \\ w_1 \end{bmatrix} = A_g \begin{bmatrix} U_1 \sin(\varphi + \psi) \\ -V_1 \cos(\varphi + \psi) \\ W_1 \sin(\varphi + \psi) \end{bmatrix}, \tag{29}$$

where A_g is the amplitude of the deformation of resonator under the effect of acceleration; ψ is the orientation of the acceleration effect; U_1, V_1, and W_1 are Rayleigh Functions, the form of which is shown as follows:

$$\begin{aligned} U_1 = V_1 &= \sin\theta \tan\left(\frac{\theta}{2}\right), \\ W_1 &= -(1 + \cos\theta) \tan\left(\frac{\theta}{2}\right). \end{aligned} \tag{30}$$

5. Simulation Analysis

Under the effect of acceleration, a relative displacement occurs between the resonator and the excitation electrode in external base, which leads to the changes of the integral domain in (18) and the initial electrode clearance d, making the change of exciting coefficients K_{c0}, K_{s0}, K_{c45}, and K_{s45}. Known from (19), when K_{s0}, K_{c45} are not zeros, amplitude stability loop and rate loop couple, and the zero drift of gyro occurs, while the variation of the K_{c0}, K_{s45} will cause changes in the gyro scale factor.

Because of the complexity of the transcendental equation and double integral analytical solution, the method of numerical calculation is used to research the exciting coefficient errors, and the process of establishment of the simulation system is as follows.

(1) Deformation caused by acceleration: A_g is changing from 0.01 μm to 0.1 μm, the interval is 0.01 μm, and ψ is changing at the range of 0° ~360°; then the interval is 10°. The deformations u_1, v_1, and w_1 caused by acceleration in (29) can be calculated.

Table 2: Simulation parameters.

Name	Parameter value	Mane	Parameter value
A_a	4 μm	ε_0	8.85×10^{-12} F/m
ϑ	0°	R	15 mm
ω_2	4 kHz	h	0.5 mm
d_0	100 μm	R_{in}	15.6 mm
Grid width	0.5°	Step interval	5 μs

(2) Calculation of vibration deformation: given the amplitude A_{av} of second-order resonance state of resonator and the vibration mode angle ϑ, using (27), u_2, v_2, and w_2 can be calculated.

(3) Discretization: meshing the spatial domain of $F_1 \sim F_8$ vibration pickup, respectively (as shown in Table 1).

(4) Calculation of capacitance clearance and integral range:

(i) Quasi-Newton method is used to calculate the numerical solution of R_d at each grid point in (26) and corresponding range of latitude and longitude of exciting electrode after deformation; in (26) u, v, and w contain deformations u_1, v_1, and w_1 caused by acceleration;

(ii) the capacitance clearance at each point can be calculated by (23).

(5) Calculation of exciting coefficients K_{c0}, K_{s0}, K_{c45}, and K_{s45}:

(i) calculate K_{ci}, K_{si} using (18);

(ii) calculate the exciting coefficient in Schemes a, b, and c in the form of combination of (15)~(17).

Analyzing the effect of acceleration on incentive system is the analysis of the relationship between A_g, ψ in (26) and the exciting coefficients K_{c0}, K_{s0}, K_{c45}, and K_{s45}. The simulation system parameter is set as Table 2 showed; implement the simulation process and calculate the exciting coefficients and compare the solutions to the ideal value of the no-deformation circumstance; then the exiting coefficient errors can be acquired in Schemes a, b, and c, shown as Figures 4, 5, and 6.

It can be known from the harmonic analysis of the 10 curves shown in Figure 4 (only give the results because of more data) that the two times with the second-order harmonic coefficient of errors is equal to the amplitude of the exciting coefficient error in Scheme b, which proves that Scheme b can compensate for the first-order of the exciting coefficient error in Scheme a. In Scheme b, the constant component is amplified two times, but comparing with the first-order harmonic amplitude, the constant component is small, so it greatly weakens the exciting coefficient errors caused by acceleration in Scheme b.

It can be seen from Figure 6 that Scheme c compensates for the second-order harmonic component of Scheme b, and the constant component is amplified. While the scale of the

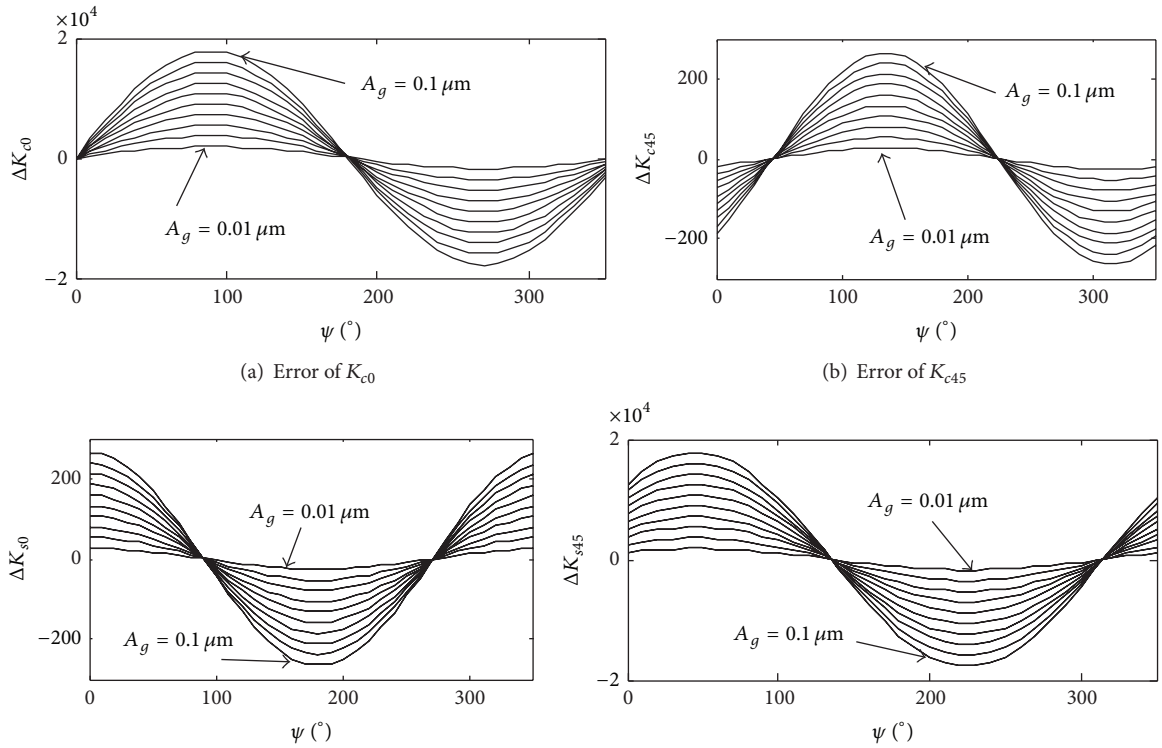

(a) Error of K_{c0}

(b) Error of K_{c45}

(c) Error of K_{s0}

(d) Error of K_{s4}

Figure 4: Exciting coefficients errors in Scheme a.

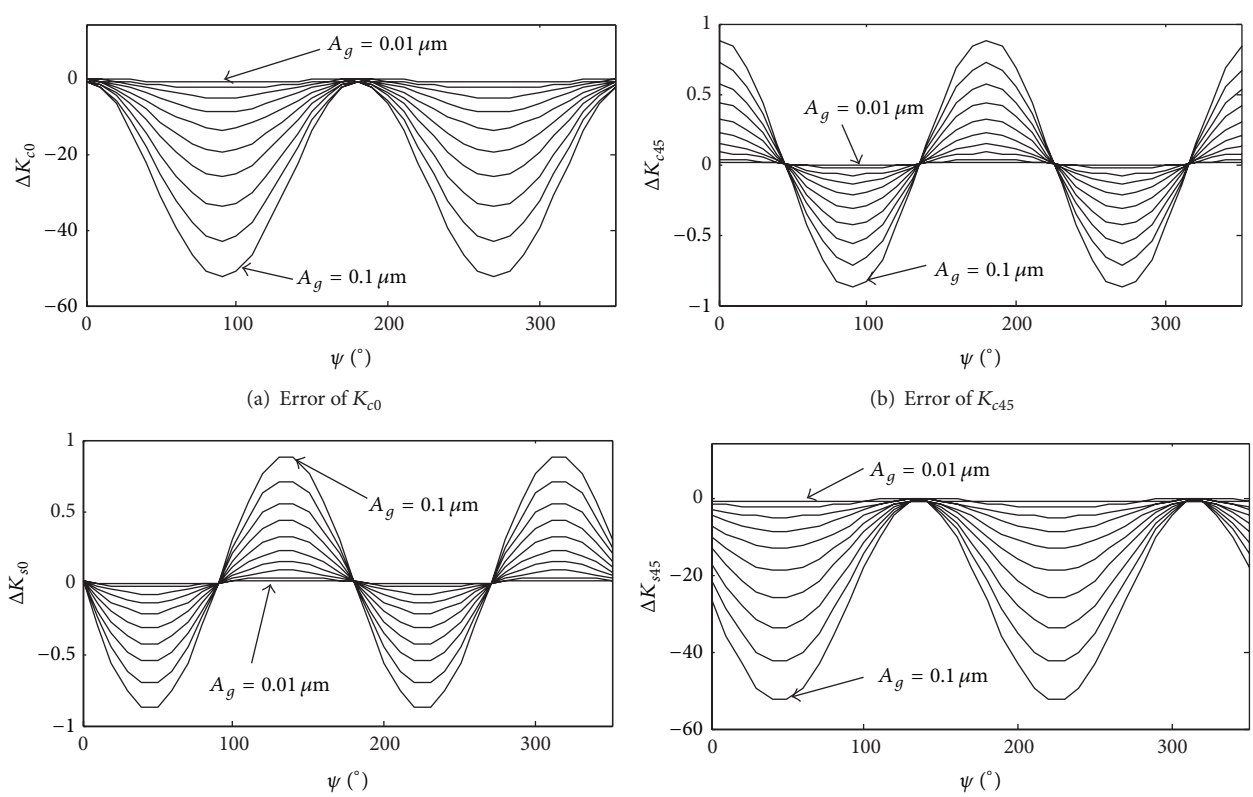

(a) Error of K_{c0}

(b) Error of K_{c45}

(c) Error of K_{s0}

(d) Error of K_{s45}

Figure 5: Exciting coefficients errors in Scheme b.

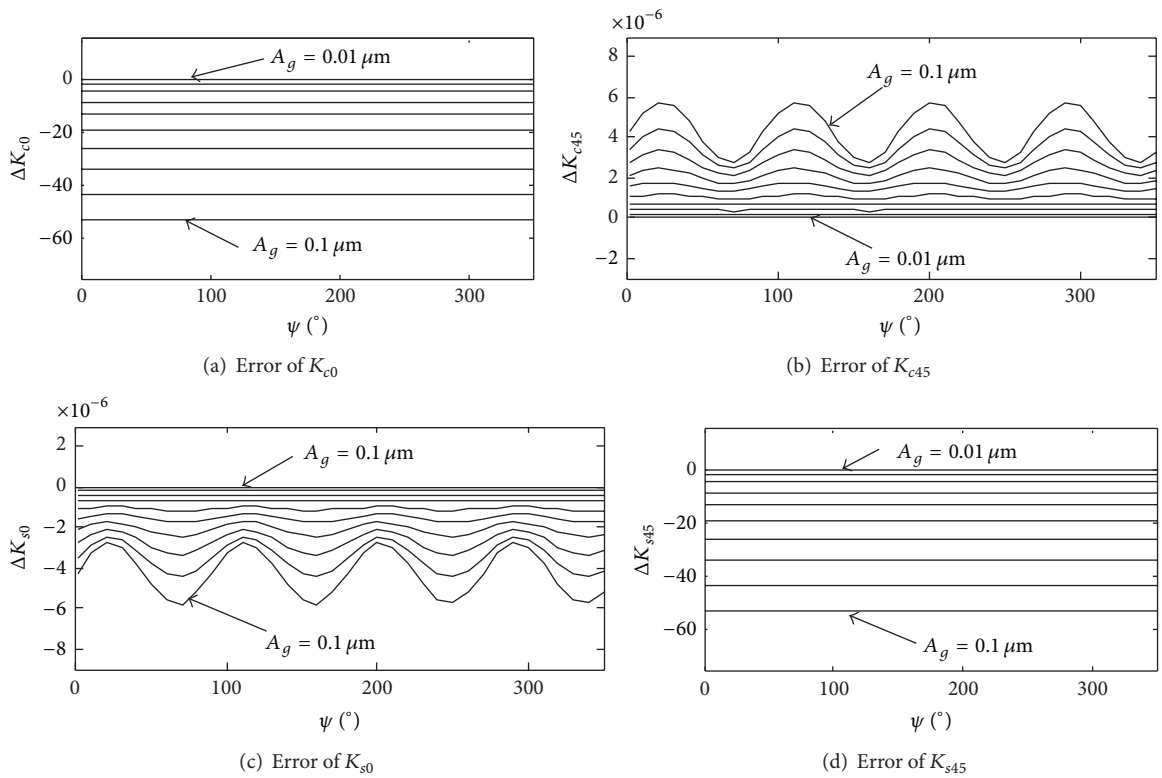

Figure 6: Exciting coefficients errors in Scheme c.

exciting coefficient error comparing to the ideal value is small, Scheme c is considered to completely eliminate the excitation system errors caused by the acceleration.

6. Conclusions

The dynamic characteristics of the HRG resonator in the condition of multielectrode incentive are researched in this paper, and the reason for causing the exciting errors by acceleration is analyzed. 3 schemes for incentive are suggested and the influences of acceleration on the deformation of the resonator in the 3 schemes are analyzed, respectively; the conclusions are as follows.

(1) The acceleration has the greatest impacts on the excitation system in Scheme a, and the error must be considered in the analysis of the drift of HRG caused by acceleration, and the bias and the scale factor are all influenced after deformation of resonator.

(2) Scheme b greatly weakens the acceleration effect on incentive system. Comparing to Scheme a, the error is reduced to the original 10^{-3} orders of magnitude.

(3) Scheme c can "completely" eliminate the acceleration effect on incentive system, so Scheme c is an ideal plan from the angle of the resistance to the impacts of acceleration.

Conflict of Interests

The authors declare that there is no conflict of interests regarding the publication of this paper.

References

[1] J. Dickinson and C. R. Strandt, "HRG strapdown navigator," in *Proceedings of the Position Location and Navigation Symposium (IEEE PLANS '90)*, pp. 110–117, Las Vegas, Nev, USA, March 1990.

[2] A. D. Meyer and D. M. Rozelle, "milli-HRG inertial navigation system," in *Proceedings of the IEEE/ION Position, Location and Navigation Symposium (PLANS '12)*, pp. 24–29, Myrtle Beach, SC, USA, April 2012.

[3] A. Matthews and F. J. Rybak, "Comparison of hemispherical resonator gyro and optical gyros," *IEEE Aerospace and Electronic Systems Magazine*, vol. 7, no. 5, pp. 40–46, 1992.

[4] D. M. Rozelle, "The hemispherical resonator gyro: from wineglass to the planets," in *Proceedings of the 19th AAS/AIAA Space Flight Mechanics Meeting*, pp. 1157–1178, February 2009.

[5] V. A. Matrveev, V. I. Lipatnikov, and A. V. Alekin, *Design of the Solid State Wave Gyro*, National Defense Industry Press, Beijing, China, 2009.

[6] X.-G. Zhou, L.-X. Wang, and Q. She, "Acceleration consequence analysis of HRG and experiment research," *Chinese Journal of Scientific Instrument*, vol. 29, no. 4, pp. 237–241, 2008.

[7] Y. K. Zhbanov, "Self-tuning contour of quadrature suppression in a hemispherical resonator gyroscope," *Giroskop. Navigation*, vol. 2, pp. 37–42, 2007.

[8] Y. K. Zhbanov and V. P. Zhuravlev, "Effect of movability of the resonator center on the operation of a hemispherical resonator gyro," *Mechanics of Solids*, vol. 44, no. 3, pp. 851–859, 2007.

[9] Y. K. Zhbanov, "Amplitude control contour in a hemispherical resonator gyro with automatic compensation for difference in Q-factors," *Mechanics of Solids*, vol. 43, no. 3, pp. 328–332, 2008.

[10] W. S. Watson, "Vibratory gyro skewed pick-off and driver geometry," *Journal of Micro Machines*, vol. 4, no. 10, pp. 171–179, 2010.